Solvation structure around ruthenium(II) tris(bipyridine) in lithium halide solutions

Ida Josefsson,[1] Susanna K. Eriksson,[2] Håkan Rensmo,[2] and Michael Odelius[1,a)]
[1]*Department of Physics, Stockholm University, AlbaNova University Center, SE-106 91 Stockholm, Sweden*
[2]*Department of Physics and Astronomy, Uppsala University, Box 530, SE-752 21 Uppsala, Sweden*

(Received 25 September 2015; accepted 30 December 2015; published online 12 January 2016)

The solvation of the ruthenium(II) tris(bipyridine) ion ($[Ru(bpy)_3]^{2+}$) is investigated with molecular dynamics simulations of lithium halide solutions in polar solvents. The anion distribution around the $[Ru(bpy)_3]^{2+}$ complex exhibits a strong solvent dependence. In aqueous solution, the iodide ion forms a solvent shared complex with $[Ru(bpy)_3]^{2+}$, but not in the other solvents. Between Cl^- and $[Ru(bpy)_3]^{2+}$, the strong hydration of the chloride ion results in a solvent separated complex where more than one solvent molecule separates the anion from the metal center. Hence, tailored solvation properties in electrolytes is a route to influence ion-ion interactions and related electron transfer processes. [http://dx.doi.org/10.1063/1.4939898]

I. INTRODUCTION

The ruthenium(II) tris(bipyridine) cation ($[Ru(bpy)_3]^{2+}$) is a prototypical metallo-organic complex, which belongs to the important class of pyridine-based transition metal complexes with numerous applications in functional materials. In particular, in the field of dye-sensitized solar cells (DSCs),[1] the solvation of ruthenium dyes in different solvents and electrolytes has been studied intensely. The iodide/triiodide redox couple acts as a hole conductor in the original realization by O'Regan and Grätzel[1] of a liquid electrolyte DSC, in which it effectuates the regeneration of the photo-oxidized dye. The mechanism for the regeneration reaction by the I^-/I_3^- redox couple is not fully understood, and whether the reaction is first or second order in I^- is a debated aspect. It has been shown that the mechanism for electron transfer involves complexation of iodide to the ruthenium dye.[1–5] In order for the iodine based redox couple to transfer an electron rapidly to an oxidized dye cation in the dye-sensitized solar cell, the distance between the reactants must be sufficiently short to favor interaction between I^- and the reaction site in the metal complex. If the distance between I^- and the metal complex is short even before the photooxidation, the rate for regeneration can more easily compete with the back transfer of the injected electron.

To understand the solvent dependence in the solar cell efficiency, it is important to investigate the ion–ion interaction in relevant systems. The interactions of ruthenium polypyridyl complexes with counterions have been carefully studied.[6–8] Acetonitrile and similar solvents have frequently been used in high-efficiency configurations of the DSC, but water impurities are difficult to avoid, partly due to problems associated with creating a durable sealing of the solar cells. Furthermore, for environmental and cost reasons, solar cells based on aqueous solutions are of particular interest.[9]

a)Author to whom correspondence should be addressed. Electronic mail: odelius@fysik.su.se. URL: http://www.fysik.su.se/~odelius

The $[Ru(bpy)_3]^{2+}$ complex is a suitable model system for investigating the optical and excited state properties of ruthenium polypyridyl complexes in solution, which have been extensively studied with a broad range of spectroscopic techniques over several decades[10–12] and by theoretical studies.[13–16] The theoretical approaches also involve molecular dynamics (MD) simulations to simulate the hydration structure, ultra-fast excited-state dynamics, and redox properties.[17–19]

Our classical MD simulation study can be viewed as an extension of this work focusing on the solvent dependence and the interaction with counterions, in particular with the iodide ion. The general structures obtained by the theoretical models are important for understanding the details about electron transfer processes in energy related applications such as the DSC.

A. Molecular dynamics simulations

We have used classical MD simulations to study the solvation of $[Ru(bpy)_3]^{2+}$ in a series of polar solutions and its interaction with halide anions. The MDynaMix code[20] was used to run classical MD simulations of $[Ru(bpy)_3]^{2+}$, Li^+, Cl^-, and I^- ions in aqueous, ethanol, and acetonitrile solutions, which are polar solvents with and without hydrogen bonding.

The simulation cells contained 3200 solvent molecules, 8 Ru-complexes, 64 anions, and 48 Li^+ for overall charge neutrality. The composition corresponds to $[Ru(bpy)_3]^{2+}$ concentrations in the range of 0.04–0.12M in various solutions. For each solvent, three solutions were simulated: two solutions with either purely Cl^- anions or purely I^- anions and a mixture with equal parts of Cl^- and I^-. The simulations were performed in the canonical ensemble (NVT), using periodic boundary conditions, with the densities kept fixed at the pure solvent densities under standard ambient conditions ($\rho_{water} = 1.00\,g/cm^3$, $\rho_{ethanol} = 0.79\,g/cm^3$, and $\rho_{acetonitrile} = 0.79\,g/cm^3$). The simulation boxes were cubic, with box lengths in the mixed ion solutions of 48.3 Å (water), 66.7 Å (acetonitrile), and 69.6 Å (ethanol), determined by the density. The use of pure solvent densities throughout the simulations was justified by a comparison of densities obtained from simulations of the aqueous solutions at constant temperature and pressure (NpT) with the density of pure water. In NpT simulations, the force fields gave moderately higher densities—1.04 g/cm^3 (Cl^- ions) and 1.09 g/cm^3 (I^- ions)—but the difference is deemed too small to explain the different behaviour in solvation presented below.

The simulations are based on simple non-polarizable force fields. The solvents were represented using the flexible simple point charge (SPC) water[21] model, OPLS-AA parameters for ethanol,[22] and a six-site acetonitrile model,[23] respectively. The force field parameters for the $[Ru(bpy)_3]^{2+}$ ion and the intermolecular parameters for Li^+, Cl^-, and I^- were also taken from the literature.[17,24] The force field parameters are reported in Appendix C. The Lorentz–Berthelot combination rules[25,26] were used for different Lennard–Jones parameters, except for in the simulations of ethanol solution, where the σ parameter was calculated as a geometrical average of two different types.

A multiple time step algorithm[27] was employed, with a short time step of 0.2 fs to describe the fast vibrational degrees of freedom, updating only intramolecular interactions and short-range (up to 5 Å) intermolecular interactions. The long-range intermolecular interactions were integrated after every 2.0 fs. Long-range electrostatic interactions were treated with Ewald summation,[28] with the cutoff distance in real space $R_{cut} = 12.0$ Å and the Ewald parameter $\alpha = 2.8R_{cut}$. The temperature was kept at 298 K by a Nosé thermostat[29] with a relaxation time of 30 fs. Data were collected during 1 ns after $\geq$300 ps equilibration for each solution. Diffusion coefficients were checked to ensure that the solutions were liquid.

In order to analyze the solvation structure, we calculated radial distribution functions (RDFs) from the MD trajectories. The RDFs (also denoted $g(r)$) contain information on the probability density of finding a specific atom type at a separation by the distance r around a given central atom, relative to a uniform distribution a the same density, and can hence be directly related to solvation shells around an ion. Since the RDF is orientationally averaged over the angular coordinates, more details in the local solvation structure are not captured. Therefore, the three-dimensional density distribution of ions and molecules around the Ru

complex was also described with spatial distribution functions (SDFs), which span both the radial and angular parts of the separation between the atoms, with respect to a local coordinate system centered on the $[Ru(bpy)_3]^{2+}$ complex and following its reorientation.

II. RESULTS

In the presentation of the structural analysis, we start with the distribution of ions around the $[Ru(bpy)_3]^{2+}$ complex, which is the core of the study. The distribution of halide ions is then rationalized in terms of the solvent distribution around both the metal complex and the halide ions.

A. The radial distribution of halide anions around the Ru center

In Figure 1, the radial distribution of halide and lithium ions around the Ru(II) center is presented for three solutions of each solvent. The solutions with either purely iodide counterions or purely chloride counterions are compared with the solution with equal concentrations of the halide anions. The ratio of $[Ru(bpy)_3]^{2+}$ and halide ions was 1:8 in all solutions. The RDFs show two well-defined configurations of halide ions around the $[Ru(bpy)_3]^{2+}$ complex, giving

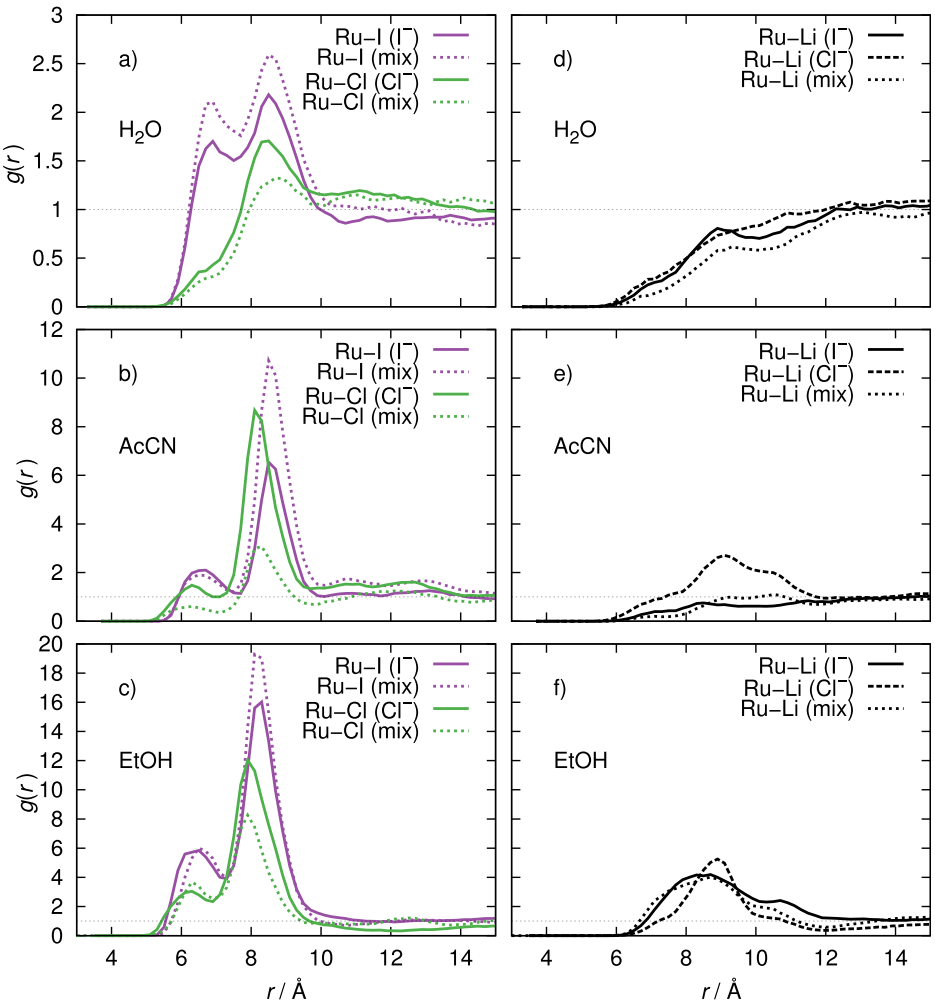

FIG. 1. Left: Radial distribution functions (RDFs) between the Ru(II) center in $[Ru(bpy)_3]^{2+}$ and halide ions in water (H_2O), acetonitrile (AcCN), and ethanol (EtOH) solutions. The results from simulations with a single type of halide ions are presented as solid lines, whereas dashed lines refer to the halide mixtures. Right: RDFs between Ru(II) and Li^+ for which the halide solutions are distinguished by I^- (solid), Cl^- (long dash), and mixed counterions (short dash).

rise to features in the RDFs at different distances. We will begin with the analysis of the iodide distribution.

In aqueous solutions, presented in panel (a) in Figure 1, the Ru–I RDF show two distinct maxima, corresponding to regions with high I^- density around the metal center: the first at 6.9 Å Ru–I separation and the second at 8.5 Å away from the metal center.

In contrast, the Ru–Cl RDF from the corresponding aqueous simulation containing only Cl^- anions lacks a region with high Cl^- density close to the metal. However, at the same distance from the Ru-center as the outermost Ru–I maximum, a peak of comparable but slightly smaller magnitude is found.

The Ru–I RDF from an aqueous solution with equal molar concentrations of both anions, represented by a dashed line in Figure 1, is similar to the RDF for the single-type anion solution, but shows an increased relative concentration at the regions of high I^- density. Consistent with the increase in I^-, the Cl^- density at the position of the first maximum is substantially decreased with respect to the solution with only Cl^- ions present: For the mixed solution, the Ru–Cl RDF value at the maximum at close to 9 Å is only slightly higher than the average Cl^- bulk concentration, indicated by a dashed line in Figure 1.

The inner solvation, resulting in solvent-shared ion pairs, is strongly suppressed for Cl^-, and Ru(II)–halide association is hence an I^- selective process. The averages of the number of ions $n(r)$ in the high density regions are given in Appendix B.

How does then the anion distribution in aqueous solution compare with the other solvents? The Ru–I and Ru–Cl RDFs for acetonitrile and ethanol solutions, presented in panels (b) and (c) in Figure 1, respectively, both have two clear maxima. In contrast, the first maximum is not pronounced for aqueous solution, but solvent-shared association is present.

The distance to the second maximum decreases systematically in the vertical series, whereas the first maximum is not as pronounced for aqueous solution and exhibits a weaker solvent dependence in acetonitrile and ethanol solutions. Since solvation shells around the halide ions in acetonitrile and ethanol are less pronounced than in water, it is possible also for Cl^- to come close to Ru(II). We observe a dramatic increase in the peak maxima with decreasing dielectric constant ϵ of the solvent: water ($\epsilon = 78$) < acetonitrile ($\epsilon = 37$) < ethanol ($\epsilon = 25$). The large amplitude of $g(r)$ in acetonitrile and ethanol is a signature of ion-pairing, occurring due to insufficient screening of the Coloumbic interaction between the ions. The ability to form Ru–halide ion pairs is the highest in ethanol, which has the smallest dielectric constant. The average number of Ru–halide ion pairs during the simulation, shown in Table I, is the largest in ethanol solution. In comparison with water, charges are less screened in acetonitrile solution. Despite the stronger ion–ion interaction in acetonitrile solution, the number of halide ions associating with the Ru complex is lower, since ion association in acetonitrile solution is confined to a small solid angle about the $[Ru(bpy)_3]^{2+}$ complex.

In solutions with equal amounts of solvated I^- and Cl^- anions (dashed lined in the left panels in Figure 1), the relative concentration of I^- anions close to the metal increases with respect to solutions containing a single anion type, while the Cl^- concentration decreases. Hence, in the mixed I^- /Cl^- solutions, the I^- ion is preferentially solvating the $[Ru(bpy)_3]^{2+}$ complex in all solvents. Since the halide ions interact less strongly with surrounding acetonitrile and ethanol molecules than with water, none of the halides have a strong solvation shell in acetonitrile and ethanol. Nothing thus prevents it from approaching the Ru complex, and it is possible for Cl^- also to enter between the ligands. We notice, however, that the ratio between the first and second peaks is lower than in the Ru–I RDF from the water simulation, indicating that the bulkier solvent molecules to some extent block the halide anions from penetrating the outer solvation shell.

In panels (e) and (f) in Figure 1, the radial distribution of lithium ions around the Ru(II) center is presented. In aqueous solutions, the lithium ions generally avoid the $[Ru(bpy)_3]^{2+}$ complex as expected since the positive charges of cations repel each other. However, in ethanol, there is a broad coordination peak resulting from the attractive interaction with the halide anions, which are located close to the Ru complex with high probability. In acetonitrile, the situation is more complicated, since there is a strong solvent dependence and a cation-cation

TABLE I. Average number of halide ions in the RDF peaks in Figure 1 during the simulations of solutions containing either I^- or Cl^- (single) or both types of anions (mixed).

			H_2O			
	Solvent shared			Solvent separated		
	Ru–ion distance	$n(r)$, single	$n(r)$, mixed	Ru–ion distance	$n(r)$, single	$n(r)$, mixed
I^-	$r \leq 7.5$ Å	0.74	0.47	$7.5 < r \leq 10.1$ Å	2.22	1.37
Cl^-	$r \leq 7.1$ Å	0.15	0.05	$7.1 < r \leq 10.1$ Å	2.22	0.88
			CH_3CN			
	Solvent shared			Solvent separated		
	Ru–ion distance	$n(r)$, single	$n(r)$, mixed	Ru–ion distance	$n(r)$, single	$n(r)$, mixed
I^-	$r \leq 7.5$ Å	0.36	0.17	$7.5 < r \leq 10.1$ Å	1.61	1.31
Cl^-	$r \leq 7.1$ Å	0.22	0.05	$7.1 < r \leq 9.9$ Å	2.09	0.41
			C_2H_5OH			
	First peak			Second peak		
	Ru–ion distance	$n(r)$, single	$n(r)$, mixed	Ru–ion distance	$n(r)$, single	$n(r)$, mixed
I^-	$r \leq 7.3$ Å	0.86	0.41	$7.3 < r \leq 9.9$ Å	3.35	1.91
Cl^-	$r \leq 6.9$ Å	0.39	0.18	$6.9 < r \leq 9.9$ Å	2.74	0.89

coordination only occurs in the simulation with only Cl^- anions. It has been reported in studies of aqueous sodium sulfate solutions by Wernersson and Jungwirth[30] that non-polarizable force fields can give an unrealistically large degree of ion pairing and clustering, a problem which can be improved with polarizable models. Hence, we assign the cation-cation attraction to an interaction mediated by the halide ions, which might be overestimated in the current force field models. Further investigations with improved force fields are required to quantify the ion pairing. However, the qualitative conclusions derived from the present simulations result from the distinctly different solvent properties due to electrostatic interactions and are thus deemed reliable.

In conclusion, we observe a strong solvent dependence in the distribution of anions around the $[Ru(bpy)_3]^{2+}$ complex. We can identify two modes of coordination with different distances (6–7 Å and 8 Å) to the Ru(II) center. We also observe a strong selectivity between I^- and Cl^- in the coordination. To rationalize the structural information contained in the RDFs in Figure 1, we need to analyze the solvent structure around the ions.

B. Solvation structures

The RDFs of the different solvents around the $[Ru(bpy)_3]^{2+}$ complex is presented in Figure 2. Before going into the analysis of each solvent, we notice that the anion substitution, in general, has only a small influence on the solvent distribution around the Ru(II) center. The largest difference is that in the presence of the Cl^- ion, the coordination of oxygen around ruthenium is more pronounced than for the solutions with I^- ions, indicative of a strong chloride–oxygen interaction.

We will begin by analyzing the hydration structure around the $[Ru(bpy)_3]^{2+}$ complex which has been described earlier in QM/MM simulations of the aqueous solution.[17] The two distinct oxygen (and hydrogen) RDF maxima at the Ru–O distances of 5.9 Å and 7.9 Å in panel (a) in Figure 2 can be interpreted as two hydration shells, shielding the complex. In a previous study

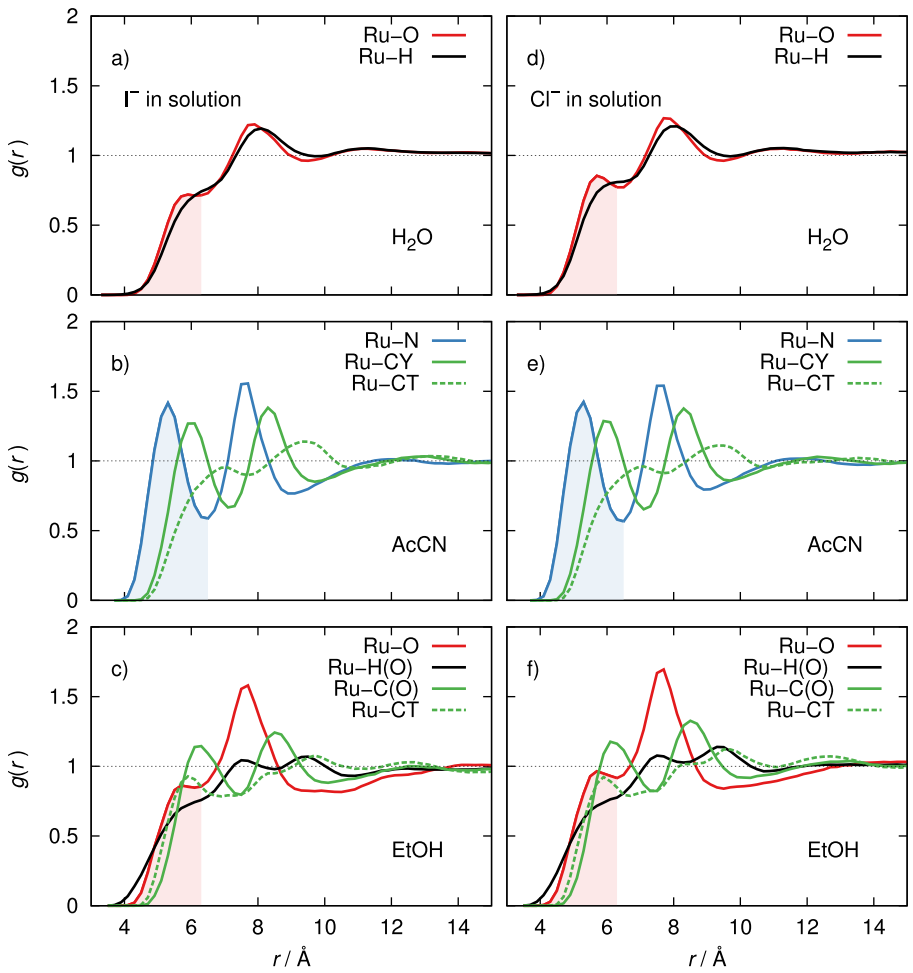

FIG. 2. RDFs between the Ru(II) center and atoms in the solvent molecules. Left: solutions with I^- anions only. Right: solutions with Cl^- anions only. The shaded regions in the Ru–solvent RDFs represent the solvent site coordinating the metal in the first solvation shell: oxygen (O) or nitrogen (N). The outer boundary of the solvation shell is defined by the first minimum in the Ru–O/Ru–N RDF. The next RDF maximum, at larger distance from the metal, corresponds to the second solvation layer.

of $[Ru(bpy)_3]^{2+}$ in water, Moret *et al.*[17] show that the first O + H peak in Figure 2 corresponds to water molecules aligning themselves in a symmetrical pattern in the grooves between the bipyridine ligands and along the three-fold symmetry axis of the $[Ru(bpy)_3]^{2+}$ complex, with oxygen coordinating the Ru atom. With the weakly defined outer boundary of the first hydration shell taken to be a Ru–O distance of 6.3 Å, we deduce that there are 12 water molecules in the first shell. This coordination number varies between 9 and 16 water molecules (varying the distance criterion between 6.1 and 6.5 Å) in the three solutions with different anion composition, for which the RDFs are given in Figure 7. For comparison, a coordination number of 15 is reported in the earlier simulations.[17]

With respect to the Ru center, the second shell is formed about 1.5 Å above the first hydration layer. More illuminating details of the hydration structure can be extracted from the three-dimensional SDFs in Figure 3, which show that the water molecules in the second shell cover the bipyridine ligands rather than the hydrogen bonded chain of solvent molecules in the first hydration layer. There is also a weakly ordered third hydration shell at about 11 Å from the complex center, most pronounced above the first solvation shell, but not intercalating between the bipyridine ligands. (The distance from the Ru(II) center to the most external hydrogen atoms on the ligands is about 6 Å.)

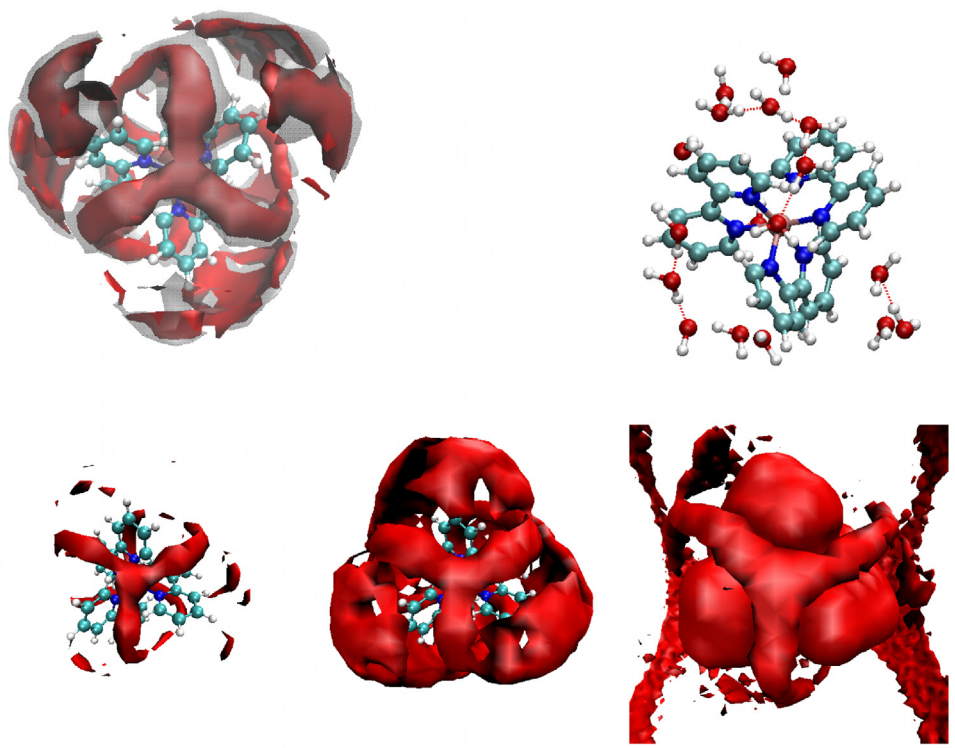

FIG. 3. Top row: Spatial distribution functions of water oxygen (red) and hydrogen (transparent gray) versus the $[Ru(bpy)_3]^{2+}$ ion in aqueous solution. The first maxima in the Ru–O and Ru–H RDFs in Figure 2 correspond to the closest maximum on the isosurface (in between the ligands), while the second peak in the RDF corresponds to a region of high probability of water molecules covering the ligands. Bottom row: Isosurfaces of the spatial distribution function of water oxygen with respect to $[Ru(bpy)_3]^{2+}$. Left: First hydration shell. Center: first + second hydration shell. Right: first + second + third hydration shell.

In the middle and bottom panels in Figure 2, we present the solvent distribution for the atomic sites in the AcCN and EtOH molecules around the Ru(II) center. The position of the first Ru–C RDF maxima for acetonitrile and ethanol in panels (b), (c), (e), and (f) in Figure 2 coincide with the first Ru–halide maxima in corresponding panels in Figure 1, while a greater fraction of halide ions approaching the metal complex in aqueous solution are able to access the area between the ligands. The number of solvent molecules integrated over the first solvation sphere, defined by the first minimum in the Ru–N RDF at 6.5 Å Ru–N separation, was found to be 8. For ethanol, we defined the solvation shell boundary by a Ru–O separation of 6.2 Å, and the average number of solvent molecules in the first shell was 5 (average of 3 simulations: 4–6 molecules and first minimum at 6.1–6.3 Å). In Figure 4, we observe that for acetonitrile and ethanol the first solvation shell around the $[Ru(bpy)_3]^{2+}$ complex form similar chains as water, and the second layer of AcCN/EtOH molecular is covering the ligands, just like in aqueous solution. However, the first and second Ru–N solvation shells are more separated than the corresponding Ru–O solvation shells in water and ethanol. Hence, it impossible to define a clear separation between the two Ru–O solvation shells, and the estimates of coordination numbers in water and ethanol are approximate. The strong interaction between solvent molecules in the two shells is governed by hydrogen bonding in water and ethanol.

C. Distribution of anions relative to the solvent around the $[Ru(bpy)_3]^{2+}$ complex

Given the analysis of the solvent distribution around the $[Ru(bpy)_3]^{2+}$ complex, we have now established a framework for understanding the anion distribution around the Ru(II) center. Beginning with the aqueous solution, we notice that the first maximum in the I–Ru RDF in the top-left panel in Figure 1, at 6.9 Å Ru–I separation, is found between the two first hydration

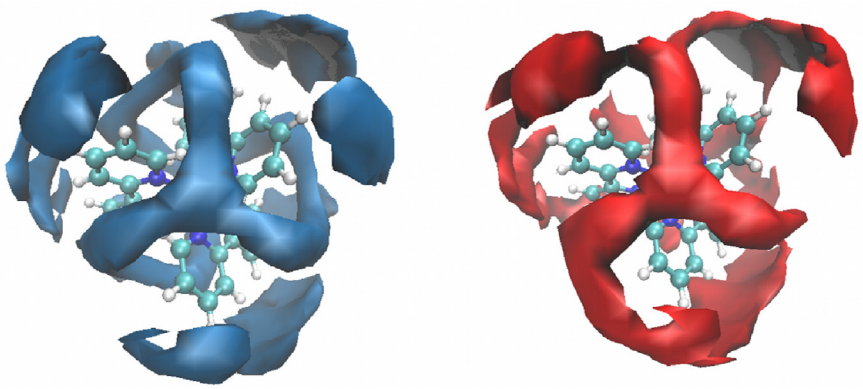

FIG. 4. Spatial distribution functions in acetonitrile and ethanol solution. N in blue (left) and O in red (right).

shells in the Ru–water RDFs, with the second region of high I^- density immediately outside the second hydration shell. The Cl^- distribution has a maximum outside the second shell, but the probability of finding Cl^- inside it is considerably lower than in bulk solution.

The Ru–anion SDFs in Figure 5 confirm that the I^- ions are indeed likely to come closer to the Ru(II) center, while Cl^-, despite its small radius, is most of the time located outside the hydrogen atoms in the second hydration shell above the bipyridine ligands.

III. DISCUSSION AND CONCLUSIONS

The difference in ion-pair formation between the two halide solutions can be understood in terms of how the anions are solvated. Due to the smaller size of the Cl^- anion, its surface charge density is higher, and hence it binds more strongly to the first hydration layer than I^-. It is likely that the effective size of the Cl^- solvent sphere prevents the ion from entering inside the second hydration shell of the $[Ru(bpy)_3]^{2+}$ complex, while the partly bare I^- ion is found in or just outside the first hydration shell with high probability, due to its weaker electrostatic interaction with the surrounding water molecules. As a result, the two halide anions are distributed in different regions around the $[Ru(bpy)_3]^{2+}$ complex, with the I^- positioned in-between the bipyridine ligands.

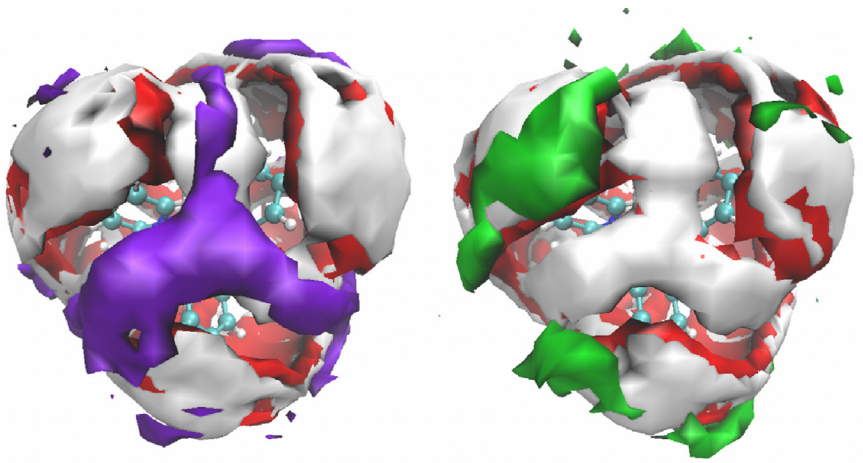

FIG. 5. I^- (violet) and Cl^- (green) spatial distribution functions with respect to $[Ru(bpy)_3]^{2+}$ in aqueous solution together with oxygen (red) and hydrogen (light gray). Immediately above the first hydration shell of $[Ru(bpy)_3]^{2+}$ between the bipyridine ligands, the density of I^- ions is high, whereas Cl^- ions are mostly found outside the outer hydration shell above the ligands.

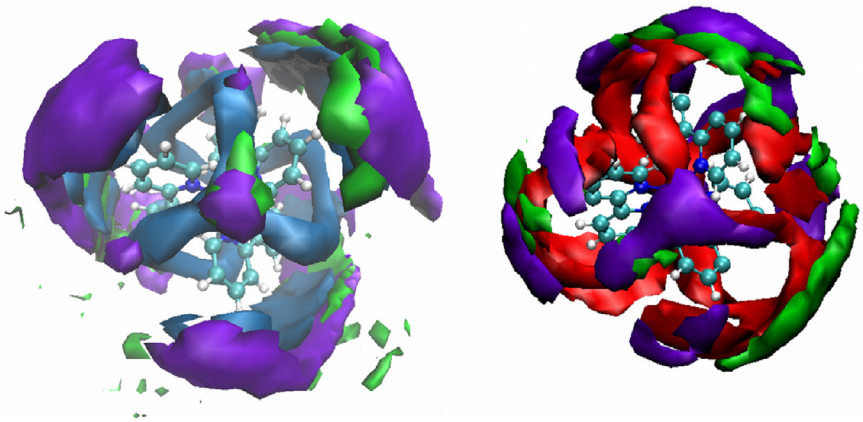

FIG. 6. I^- (violet) and Cl^- (green) spatial distribution functions with respect to $[Ru(bpy)_3]^{2+}$ in acetonitrile with nitrogen (blue) and ethanol with oxygen (red). Left: N, Cl, and I. Right: O, I, and Cl. The acetonitrile nitrogen and ethanol oxygen spatial distribution functions are similar to water oxygen, but the anions enter inside the second shell mainly along the C_3 axis, not above the meandering ethanol chain.

Also for the acetonitrile and ethanol solutions, the solvation shells around the $[Ru(bpy)_3]^{2+}$ complex giving the double maxima in the Ru–I and Ru–Cl RDFs in Figure 1 can be understood as corresponding to two different regions: one between the two first solvation layers of $[Ru(bpy)_3]^{2+}$ and the second at the outer boundary of the second solvation shell. We observe that solvent-shared Ru–halide ion-pairs (between solvation shells) are formed with the halide ions situated along the C_3 symmetry axis of $[Ru(bpy)_3]^{2+}$ (see Figure 6). In fact, the first shell of solvent-shared Ru-halide pairing occurs solely along the C_3 axis of the Ru complex in acetonitrile and ethanol. Because the bulky aliphatic groups of acetonitrile and ethanol block the region between the bipyridine ligands, the Ru–anion interaction is confined to the position along the symmetry axis, where the density of solvent molecules is low. As seen in Figures 1 and 6, this leads to a lack of anion distribution in the first shell between the bipyridine ligands. The stiffness of the bonds and angles in the classical force field of the $[Ru(bpy)_3]^{2+}$ complex may affect the short-range interaction with the solvent. However, we deem that the ion and solvent dependences that we observe are strong enough to be insensitive to the details of the intramolecular force field of the cation.

In the context of DSCs, this solvent-shared configuration would be populated already in the ground state for ruthenium polypyridyl dyes in electrolyte solution. At photo-oxidation of the dye, the solvent-shared configuration could act as a precursor state for regeneration of the dyes to enable a new photocycle. An optimal anion distribution could reduce the competing mechanism of back-transfer of the photo-excited electron. Hence, investigations of the rate of back-transfer as a function of electrolyte composition and solvent variations could be a route to improve the solar cell efficiency.

Although the concentration of halide ions inside the second solvation shell relative to the concentration of halide anions at the outer boundary of the second shell is lower in organic solvents than in aqueous solution, the halide concentrations at the high density regions are markedly higher than in aqueous solution. It is the highest for the ethanol solutions, which is expected from Coloumb's law, as the electrostatic interaction between the ions is inversely proportional to the dielectric constant ϵ of the medium. We notice that the number of solvent molecules in the first solvation shell of the $[Ru(bpy)_3]^{2+}$ complex is larger in water and acetonitrile than in ethanol solution, which results in better screening of the cation.

The solvation of the $[Ru(bpy)_3]^{2+}$ complex influences the electronic structure, and shifts the electronic energy levels which can be probed with electron spectroscopic techniques. We are planning to address the relation between solvation structure and electronic and electrochemical properties with liquid jet photoelectron spectroscopy experiments of $[Ru(bpy)_3]^{2+}$ halide solutions in the future.

ACKNOWLEDGMENTS

The work was financially supported by the Swedish Research Council (VR), the Carl Trygger Foundation, the Lars Hierta foundation, the STandUP for Energy program, and the Swedish Energy Agency. The theoretical modeling was made possible through generous allocations of computer time provided by the Swedish National Infrastructure for Computing (SNIC) at the Swedish National Supercomputer Center (NSC) and the High Performance Computer Center North (HPC2N), Sweden.

APPENDIX A: RUTHENIUM–SOLVENT RADIAL DISTRIBUTION FUNCTIONS

The Ru–solvent RDFs for the altogether nine electrolyte solutions simulated are shown in Figure 7. The first minimum in the Ru–O/N RDF defines the outer boundary of the first solvation shell. The distribution of solvent molecules does not depend strongly on the kind of anion present.

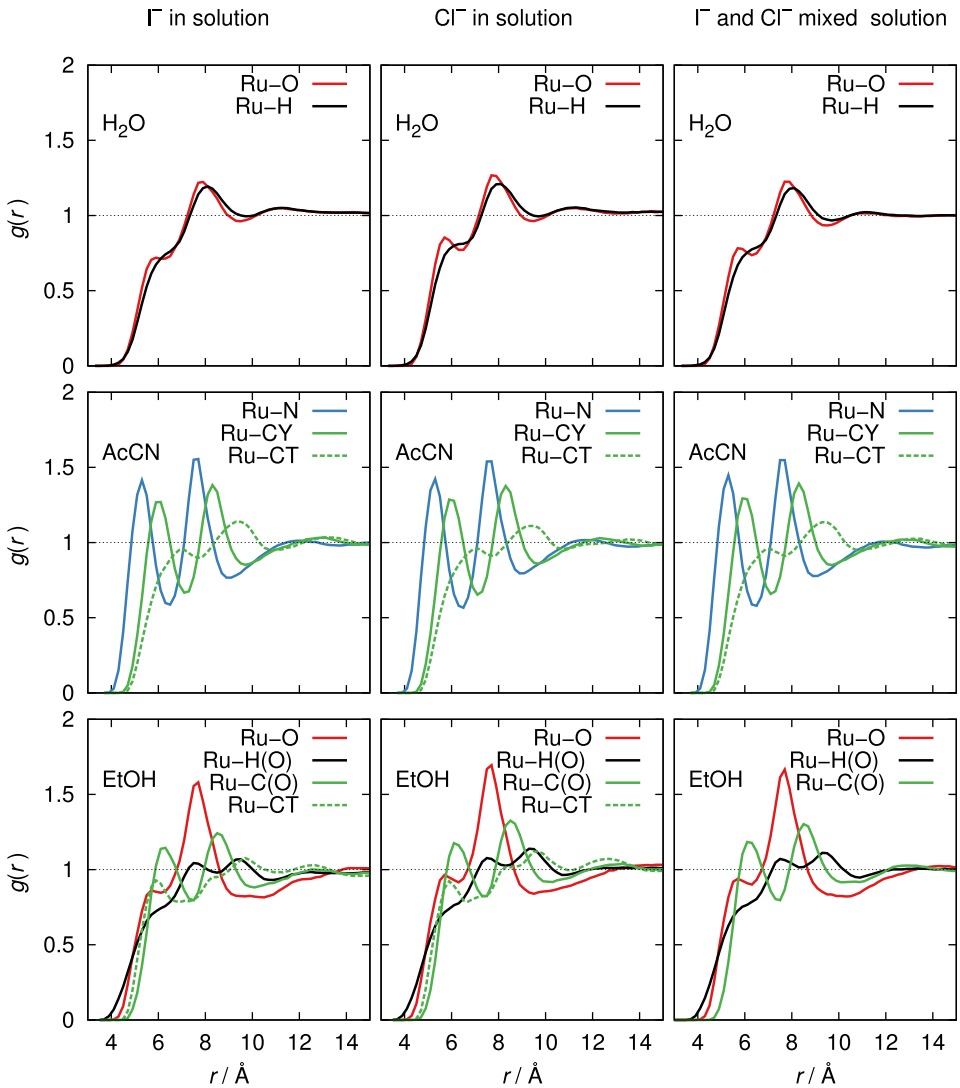

FIG. 7. Ru–solvent RDFs for solutions with I^-, Cl^-, and equal amounts of both halides solvated in water, ethanol, and acetonitrile.

APPENDIX B: COORDINATION NUMBERS OF HALIDE IONS WITH RESPECT TO Ru

Table I shows the integrated coordination numbers $n(r)$ of I^- and Cl^- with respect to the metal center of the $[Ru(bpy)_3]^{2+}$ complex. We define solvent shared ion pairs as the Ru–halide pairs giving rise to the innermost RDF peak in Figure 1 and solvent separated pairs as the Ru–halide pairs in the second peak. The interatomic separation ranges chosen for selecting the relevant regions are given in Table I.

APPENDIX C: FORCE FIELD PARAMETERS

The force field parameters for the $[Ru(bpy)_3]^{2+}$ cation,[17] Li^+ and halide anions,[24] and solvents[21–23] reported in this section were taken from the literature. The van der Waals interactions were described with a Lennard–Jones potential with the parameter ϵ describing the interaction strength and the parameter σ the interatomic distance for the potential minimum listed in Table II. The interaction energy between pairs of dissimilar atoms was calculated according to the Lorentz–Berthelot mixing rules[25,26] in the simulations of aqueous and acetonitrile solutions, and both σ and ϵ as geometrical averages in the ethanol simulations.

The partial atomic charges of $[Ru(bpy)_3]^{2+}$ were fitted to the electrostatic potential (ESP) charges in a B3LYP calculation with the DGTZVP basis set on N, C, and H and DGDZVP on Ru. Since the charges are fitted to the potential at the molecular surface, the innermost atoms (Ru and N) can get unphysical charges, but in total the charges create the electrostatic potential experienced by the solvent and ions. We observe a symmetry breaking in the derivation of ESP charges, and as a result, equivalent atoms may have different charges. The atomic charges in Table II are, however, given as the average charge on equivalent atoms, labeled according to Figure 8.

Simulations of 8 $[Ru(bpy)_3]^{2+}$, 64 halide ions, and 48 Li^+ in aqueous solution, describing the electrostatics with the calculated ESP charges on $[Ru(bpy)_3]^{2+}$ and the symmetrized charges in Table II, showed that the structural averages were not significantly affected by the charge asymmetry on $[Ru(bpy)_3]^{2+}$. The Ru–solvent RDFs were essentially unaffected by the symmetrization of the force field charges, describing electrostatic interactions with the $[Ru(bpy)_3]^{2+}$ cation. The average number of solvent-shared Ru–I ion pairs was 0.91 when the calculated ESP charges were used and 0.98 when the average of the charges on identical atoms was used. There were on average 2.21 (calculated charges) and 2.46 (averaged charges) solvent-separated Ru–I ion pairs, with the outer boundary of the ion-pair region at 10.1 Å. The number of Ru–Cl ion pairs up to an interatomic separation of 10.1 Å was 2.5 in both calculations. Extended simulations, investigating the

TABLE II. Nonbonded parameters for the solute atoms.

	Q	σ (Å)	ϵ (kJ/M)
I^-	−1.0000	5.40	0.408
Cl^-	−1.0000	4.86	0.168
Li^+	1.0000	2.37	0.149
Ru	−1.6209	2.96	2.343
N	0.3989	3.25	0.711
C2	0.0256	3.55	0.293
C3	−0.1748	3.55	0.293
C4	−0.0363	3.55	0.293
C5	−0.1246	3.55	0.293
C6	−0.1746	3.55	0.293
H3	0.1748	2.42	0.126
H4	0.1663	2.42	0.126
H5	0.1741	2.42	0.126
H6	0.1741	2.42	0.126

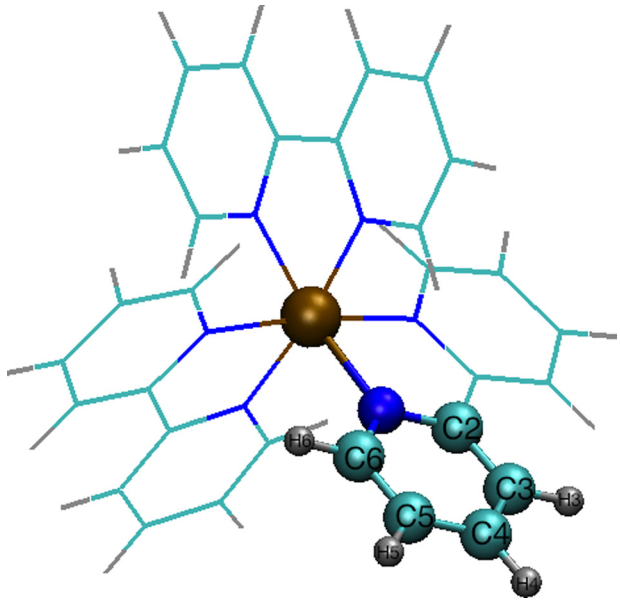

FIG. 8. $[Ru(bpy)_3]^{2+}$ with the C and H atom labels used in Table II.

error due to limited simulation length, had a similar degree of of uncertainty. The non-bonded parameters for the solvent force fields are given in Table III.

The bonded parameters for the solvents and $[Ru(bpy)_3]^{2+}$ are listed in Tables IV and V. Bond and angle potentials are harmonic, with the exception of the O–H bond of water, which is a Morse potential. The dihedral angles in ethanol were described with a MM3 potential

$$U_{\text{tors}} = K_1(1+\cos\phi)/2 + K_2(1+\cos(2\phi))/2 + K_3(1+\cos(3\phi))/2, \tag{C1}$$

whereas the $[Ru(bpy)_3]^{2+}$ dihedral potential was of the standard type

$$U_{\text{tors}} = K_\phi(1+\cos(M\phi-\Delta)). \tag{C2}$$

TABLE III. Nonbonded parameters for the simulated solvents.

	Q	σ (Å)	ϵ (kJ/M)
Water			
O	−0.8200	3.17	0.650
H	0.4100	0.00	0.000
Acetonitrile			
N	−0.5126	3.01	0.557
CY	0.4917	3.55	0.562
CT	−0.5503	3.40	0.458
HC	0.1904	2.65	0.066
Ethanol			
CT	−0.1800	3.50	0.280
C(O)	0.1450	3.50	0.280
HC	0.0600	2.50	0.130
OH	−0.6830	3.10	0.710
HO	0.4180	0.00	0.000

TABLE IV. Bonded parameters used in the simulations of solvents.

Water			
O–H[a]	$r_{eq} = 1.000$ Å	$K_r = 2811$ kJ/(mol ·Å^2)	$D = 420$ kJ/mol, $\rho = 2.566$ Å^{-1}
H–H	$r_{eq} = 1.633$ Å	$K_r = 687$ kJ/(mol ·Å^2)	
Acetonitrile			
N–CY	$r_{eq} = 1.157$ Å	$K_r = 2512$ kJ/(mol ·Å^2)	
CY–CT	$r_{eq} = 1.458$ Å	$K_r = 1675$ kJ/(mol ·Å^2)	
CT–HC	$r_{eq} = 1.090$ Å	$K_r = 1424$ kJ/(mol ·Å^2)	
N–CY–CT	$\theta_{eq} = 180.0°$	$K_\theta = 335.0$ kJ/(mol · rad^2)	
CY–CT–HC	$\theta_{eq} = 110.0°$	$K_\theta = 146.5$ kJ/(mol · rad^2)	
HC–CT–HC	$\theta_{eq} = 109.5°$	$K_\theta = 146.5$ kJ/(mol · rad^2)	
Ethanol			
CT–HC	$r_{eq} = 1.090$ Å	$K_r = 1423$ kJ/(mol ·Å^2)	
CT–CT	$r_{eq} = 1.529$ Å	$K_r = 1121$ kJ/(mol ·Å^2)	
CT–OH	$r_{eq} = 1.410$ Å	$K_r = 1339$ kJ/(mol ·Å^2)	
OH–HO	$r_{eq} = 0.945$ Å	$K_r = 2313$ kJ/(mol ·Å^2)	
HC–CT–HC	$\theta_{eq} = 107.8°$	$K_\theta = 138.0$ kJ/(mol · rad^2)	
HC–CT–CT	$\theta_{eq} = 110.7°$	$K_\theta = 157.0$ kJ/(mol · rad^2)	
CT–CT–OH	$\theta_{eq} = 109.5°$	$K_\theta = 209.0$ kJ/(mol · rad^2)	
HC–CT–OH	$\theta_{eq} = 109.5°$	$K_\theta = 146.0$ kJ/(mol · rad^2)	
CT–OH–HO	$\theta_{eq} = 108.5°$	$K_\theta = 230.0$ kJ/(mol · rad^2)	
HC–CT–CT–HC	$K_1 = 0.00$ kJ/M	$K_2 = 0.00$ kJ/M	$K_3 = 1.96$ kJ/mol
HC–CT–CT–OH	$K_1 = 0.00$ kJ/M	$K_2 = 0.00$ kJ/M	$K_3 = 1.33$ kJ/mol
CT–CT–OH–HO	$K_1 = -1.49$ kJ/M	$K_2 = -0.073$ kJ/M	$K_3 = 2.06$ kJ/mol
HC–CT–OH–HO	$K_1 = 0.00$ kJ/M	$K_2 = 0.00$ kJ/M	$K_3 = 1.88$ kJ/mol

[a]Morse potential.

TABLE V. Bonded parameters for $[Ru(bpy)_3]^{2+}$.

$[Ru(bpy)_3]^{2+}$			
Ru–NC	$r_{eq} = 2.081$ Å	$K_r = 1120.0$ kJ/(mol ·Å^2)	
NC–CA	$r_{eq} = 1.339$ Å	$K_r = 837.40$ kJ/(mol ·Å^2)	
CA–CA	$r_{eq} = 1.400$ Å	$K_r = 1964.00$ kJ/(mol ·Å^2)	
CA–HA	$r_{eq} = 1.080$ Å	$K_r = 2022.00$ kJ/(mol ·Å^2)	
NC–Ru–NC	$\theta_{eq} = 91.1°$	$K_\theta = 340.0$ kJ/(mol · rad^2)	
NC–Ru–NC	$\theta_{eq} = 180.0°$	$K_\theta = 102.47$ kJ/(mol · rad^2)	
Ru–NC–CA	$\theta_{eq} = 123.5°$	$K_\theta = 433.00$ kJ/(mol · rad^2)	
CA–NC–CA	$\theta_{eq} = 117.0°$	$K_\theta = 293.00$ kJ/(mol · rad^2)	
NC–CA–CA	$\theta_{eq} = 124.0°$	$K_\theta = 293.00$ kJ/(mol · rad^2)	
CA–CA–CA	$\theta_{eq} = 120.0°$	$K_\theta = 264.00$ kJ/(mol · rad^2)	
NC–CA–HA	$\theta_{eq} = 116.0°$	$K_\theta = 147.00$ kJ/(mol · rad^2)	
CA–CA–HA	$\theta_{eq} = 120.0°$	$K_\theta = 147.00$ kJ/(mol · rad^2)	
NC–Ru–NC–CA	$\Delta = 180.000°$	$K_\phi = 1.050$ kJ/mol	$M = 4$
Ru–NC–CA–CA	$\Delta = 0.000°$	$K_\phi = 5.060$ kJ/mol	$M = 2$
Ru–NC–CA–CA	$\Delta = 180.000°$	$K_\phi = 5.900$ kJ/mol	$M = 1$
CA–NC–CA–CA	$\Delta = 180.000°$	$K_\phi = 6.800$ kJ/mol	$M = 2$
Ru–NC–CA–HA	$\Delta = 180.000°$	$K_\phi = 22.0$ kJ/mol	$M = 2$
NC–CA–CA–NC	$\Delta = 0.000°$	$K_\phi = 4.0$ kJ/mol	$M = 2$
NC–CA–CA–HA	$\Delta = 180.000°$	$K_\phi = 1.100$ kJ/mol	$M = 2$

[1]B. O'Regan and M. Grätzel, "A low-cost, high-efficiency solar-cell based on dye-sensitized colloidal TiO_2 films," Nature **353**, 737–740 (1991).
[2]F. Schiffmann, J. VandeVondele, J. Hutter, A. Urakawa, R. Wirz, and A. Baiker, "An atomistic picture of the regeneration process in dye sensitized solar cells," Proc. Natl. Acad. Sci. U.S.A. **107**, 4830–4833 (2010).
[3]T. Liu and A. Troisi, "Theoretical evidence of multiple dye regeneration mechanisms in dye-sensitized solar cells," Chem. Phys. Lett. **570**, 159–162 (2013).
[4]A. Listorti, B. O'Regan, and J. R. Durrant, "Electron transfer dynamics in dye-sensitized solar cells," Chem. Mater. **23**, 3381–3399 (2011).
[5]A. Y. Anderson, P. R. F. Barnes, J. R. Durrant, and B. C. O'Regan, "Quantifying regeneration in dye-sensitized solar cells," J. Phys. Chem. C **115**, 2439–2447 (2011).
[6]W. M. Ward, B. H. Farnum, M. Siegler, and G. J. Meyer, "Chloride ion-pairing with Ru(II) polypyridyl compounds in dichloromethane," J. Phys. Chem. A **117**, 8883–8894 (2013).
[7]A. Marton, C. C. Clark, R. Srinivasan, R. E. Freundlich, A. A. Narducci Sarjeant, and G. J. Meyer, "Static and dynamic quenching of Ru(II) polypyridyl excited states by iodide," Inorg. Chem. **45**, 362–369 (2006).
[8]H. Kusama and K. Sayama, "A comparative computational study on the interactions of N719 and N749 dyes with iodine in dye-sensitized solar cells," Phys. Chem. Chem. Phys. **17**, 4379–4387 (2015).
[9]C. H. Law, S. C. Pathirana, X. O. Li, A. Y. Anderson, P. R. F. Barnes, A. Listorti, T. H. Ghaddar, and B. C. O'Regan, "Water-based electrolytes for dye-sensitized solar cells," Adv. Mater. **22**, 4505–4509 (2010).
[10]A. Juris, V. Balzani, F. Barigelletti, S. Campagna, P. Belser, and A. von Zelewsky, "Ru(II) polypyridine complexes: photophysics, photochemistry, eletrochemistry, and chemiluminescence," Coord. Chem. Rev. **84**, 85–277 (1988).
[11]N. H. Damrauer, G. Cerullo, A. Yeh, T. R. Boussie, C. V. Shank, and J. K. McCusker, "Femtosecond dynamics of excited-state evolution in $[Ru(bpy)_3]^{2+}$," Science **275**, 54–57 (1997).
[12]M. Saes, C. Bressler, R. Abela, D. Grolimund, S. L. Johnson, P. A. Heimann, and M. Chergui, "Observing photochemical transients by ultrafast x-ray absorption spectroscopy," Phys. Rev. Lett. **90**, 047403 (2003).
[13]C. Daul, E. J. Baerends, and P. Vernooijs, "A density functional study of the MLCT states of $[Ru(bpy)_3]^{2+}$ in D_3 symmetry," Inorg. Chem. **33**, 3538–3543 (1994).
[14]J.-L. Heully, F. Alary, and M. Boggio-Pasqua, "Spin-orbit effects on the photophysical properties of $Ru(bpy)_3^{2+}$," J. Chem. Phys. **131**, 184308 (2009).
[15]E. Ronca, F. De Angelis, and S. Fantacci, "Time-dependent density functional theory modeling of spin-orbit coupling in ruthenium and osmium solar cell sensitizers," J. Phys. Chem. C **118**, 17067–17078 (2014).
[16]M. H. Stockett and S. Brøndsted Nielsen, "Communication: Does a single CH_3CN molecule attached to $Ru(bipy)_3^{2+}$ affect its absorption spectrum?," J. Chem. Phys. **142**, 171102 (2015).
[17]M. E. Moret, I. Tavernelli, and U. Rothlisberger, "A combined QM/MM and classical molecular dynamics study of $[Ru(bpy)_3]^{2+}$ in water," J. Phys. Chem. B **113**, 7737–7744 (2009).
[18]P. Diamantis, J. F. Gonthier, I. Tavernelli, and U. Rothlisberger, "Study of the redox properties of singlet and triplet tris(2,2′-bipyridine)ruthenium(II) ($[Ru(bpy)_3]^{2+}$) in aqueous solution by full quantum and mixed quantum/classical molecular dynamics simulations," J. Phys. Chem. B **118**, 3950–3959 (2014).
[19]M. E. Moret, I. Tavernelli, M. Chergui, and U. Rothlisberger, "Electron localization dynamics in the triplet excited state of $[Ru(bpy)_3]^{2+}$ in aqueous solution," Chem. Eur. J. **16**, 5889–5894 (2010).
[20]A. P. Lyubartsev and A. Laaksonen, "M.DynaMix—A scalable portable parallel MD simulation package for arbitrary molecular mixtures," Comput. Phys. Commun. **128**, 565–589 (2000).
[21]K. Toukan and A. Rahman, "Molecular-dynamics study of atomic motions in water," Phys. Rev. B **31**, 2643–2648 (1985).
[22]W. Jorgensen, D. S. Maxwell, and J. Tirado-Rives, "Development and testing of the OPLS all-atom force field on conformational energetics and properties of organic liquids," J. Am. Chem. Soc. **118**, 11225–11236 (1996).
[23]A. M. Nikitin and A. P. Lyubartsev, "New six-site acetonitrile model for simulations of liquid acetonitrile and its aqueous mixtures," J. Comput. Chem. **28**, 2020–2026 (2007).
[24]K. Heinzinger, "Computer simulations of aqueous electrolyte solutions," Physica B+C **131**, 196–216 (1985).
[25]H. A. Lorentz, "Ueber die anwendung des satzes vom virial in der kinetischen theorie der gase," Ann. Phys. **248**, 127–136 (1881).
[26]D. Berthelot, "Sur le mélange des gaz," C. R. Acad. Sci. **126**, 1703–1706 (1889).
[27]M. Tuckerman, B. J. Berne, and G. J. Martyna, "Reversible multiple time scale molecular dynamics," J. Chem. Phys. **97**, 1990–2001 (1992).
[28]P. P. Ewald, "Die Berechnung optischer und elektrostatischer Gitterpotentiale," Ann. Phys. **369**, 253–287 (1921).
[29]S. Nosé, "A unified formulation of the constant temperature molecular dynamics methods," J. Chem. Phys. **81**, 511–519 (1984).
[30]E. Wernersson and P. Jungwirth, "Effect of water polarizability on the properties of solutions of polyvalent ions: Simulations of aqueous sodium sulfate with different force fields," J. Chem. Theory Comput. **6**, 3233–3240 (2010).